Draft version July 29, 2016
Preprint typeset using LaTeX style AASTeX6 v. 1.0

TIDAL RESPONSE OF PRELIMINARY JUPITER MODEL

Sean M. Wahl[1]
Department of Earth and Planetary Science, University of California, Berkeley, CA, 94720, USA

William B. Hubbard[2]
Lunar and Planetary Laboratory, The University of Arizona, Tucson, AZ 85721, USA

Burkhard Militzer[3]
Department of Earth and Planetary Science, University of California, Berkeley, CA, 94720, USA

[1]swahl@berkeley.edu
[2]hubbard@lpl.arizona.edu
[3]militzer@berkeley.edu; also Department of Astronomy, University of California, Berkeley, CA, 94720, USA

ABSTRACT

In anticipation of improved observational data for Jupiter's gravitational field from the *Juno* spacecraft, we predict the static tidal response for a variety of Jupiter interior models based on *ab initio* computer simulations of hydrogen-helium mixtures. We calculate hydrostatic-equilibrium gravity terms using the non-perturbative *concentric Maclaurin Spheroid* (CMS) method that eliminates lengthy expansions used in the theory of figures. Our method captures terms arising from the coupled tidal and rotational perturbations, which we find to be important for a rapidly-rotating planet like Jupiter. Our predicted static tidal Love number $k_2 = 0.5900$ is ∼10% larger than previous estimates. The value is, as expected, highly correlated with the zonal harmonic coefficient J_2, and is thus nearly constant when plausible changes are made to interior structure while holding J_2 fixed at the observed value. We note that the predicted static k_2 might change due to Jupiter's dynamical response to the Galilean moons, and find reasons to argue that the change may be detectable, although we do not present here a theory of dynamical tides for highly oblate Jovian planets. An accurate model of Jupiter's tidal response will be essential for interpreting *Juno* observations and identifying tidal signals from effects of other interior dynamics in Jupiter's gravitational field.

Keywords: giant planets, tides, Jupiter, interiors

1. INTRODUCTION

The *Juno* spacecraft began studying Jupiter at close range following its orbital insertion in early July 2016. The unique low-periapse polar orbit and precise Doppler measurements of the spacecraft's acceleration will yield parameters of Jupiter's external gravitational field to unprecedented precision, approaching a relative precision of $\sim 10^{-9}$ (Kaspi et al. 2010). In addition to providing important information about the planet's interior mass distribution, the non-spherical components of Jupiter's gravitational field should exhibit a detectable signal from tides induced by the planet's closer large moons, possibly superimposed on signals from mass anomalies induced by large-scale dynamic flows in the planet's interior (Cao & Stevenson 2015; Kaspi et al. 2010; Kaspi 2013).

As a benchmark for comparison with expected *Juno* data, Hubbard & Militzer (2016) constructed static interior models of the present state of Jupiter, using a barotropic pressure-density $P(\rho)$ equation of state for a near-solar mixture of hydrogen and helium, determined from *ab intio* molecular dynamics simulations (Militzer 2013; Militzer & Hubbard 2013). In this paper, we extend those models to predict the static tidal response of Jupiter using the three-dimensional concentric Maclaurin spheroid (CMS) method (Wahl et al. 2016).

The Hubbard & Militzer (2016) preliminary Jupiter model is an axisymmetric, rotating model with a self-consistent gravitational field, shape and interior density profile. It is constructed to fit pre-*Juno* data for the

degree-two zonal gravitational harmonic J_2 (Jacobson 2003). While solutions exist matching pre-*Juno* data for the degree-four harmonic J_4, models using the *ab initio* EOS required unphysical compositions with densities lower than that expected for the pure H-He mixture. As a result, the preferred model of Hubbard & Militzer (2016) predicts a J_4 with an absolute value above pre-*Juno* error bars. Preliminary Jupiter models consider the effect of a helium rain layer where hydrogen and helium become immiscible (Stevenson & Salpeter 1977b). The existence of such a layer has important effects for the interior structure of the planet, since it inhibits convection and mixing between the molecular exterior and metallic interior portions of the H-He envelope. This circumstance provides a physical basis for differences in composition and thermal state between the inner and outer portions of the planet. Adjustments of the heavy element content and entropy of the $P(\rho)$ barotrope allow identification of an interior structure consistent with both pre-*Juno* observational constraints and the *ab initio* material simulations. The preferred preliminary model predicts a dense inner core with ∼12 Earth masses and an inner hydrogen-helium rich envelope with ∼3× solar metallicity, using an outer envelope composition matching that measured by the *Galileo* entry probe.

Although the *Cassini* Saturn orbiter was not designed for direct measurements of the high degree and order components of Saturn's gravitational field, the first observational determination of Saturn's second degree Love number k_2 was recently reported by Lainey et al. (2016). This study used an astrometric dataset for Saturn's co-orbital satellites to fit k_2, and identified a value significantly larger than the theoretical prediction of Gavrilov & Zharkov (1977). The non-perturbative CMS method obtains values of k_2 within the observational error bars for simple models of Saturn's interior, indicating the high value can be explained completely in terms of static tidal response (Wahl et al. 2016). The perturbative method of Gavrilov & Zharkov (1977) provides an initial estimate of tidally induced terms in the gravitational potential, but neglects terms on the order of the product of tidal and rotational perturbations. Wahl et al. (2016) demonstrated, that for the rapidly-rotating Saturn, these terms are significant and sufficient to explain the observed enhancement of k_2.

2. BAROTROPE

We assume the liquid planet is in hydrostatic equilibrium,

$$\nabla P = \rho \nabla U, \tag{1}$$

where P is the pressure, ρ is the mass density and U the total effective potential. Modeling the gravitational field of such a body requires a barotrope $P(\rho)$ for the body's interior. In this paper, we use the barotrope of Hubbard & Militzer (2016), constructed from *ab initio* simulations of hydrogen-helium mixtures (Militzer 2013; Militzer & Hubbard 2013). The $P(\rho)$ relation is interpolated from a grid of adiabats determined from density functional molecular dynamics (DFT-MD) simulations using the Perdew-Burke-Ernzerhof (PBE) functional (Perdew et al. 1996) in combination with a thermodynamic integration technique. The simulations were performed with cells containing $N_{He} = 18$ helium and $N_H = 220$ hydrogen atoms, corresponding to a solar-like helium mass fraction $Y_0 = 0.245$. An adiabat is characterized by an entropy per electron $S/k_B/N_e$ (Militzer & Hubbard 2013), where k_B is Boltzmann's constant and N_e is the number of electrons. Hereafter we refer to this quantity simply as S.

In our treatment, the term "entropy" and the symbol S refer to a particular adiabatic temperature $T(P)$ relationship for a fixed composition H-He mixture ($Y_0 = 0.245$) as determined from the *ab initio* simulations. The value of S in the outer portion of the planet is determined by matching the $T(P)$ measurements from the Galileo atmospheric probe (see Figure 1). This adiabatic $T(P)$ is assumed to apply to small perturbations of composition, in terms of both helium fraction and metallicity. Hubbard & Militzer (2016) demonstrated that these compositional perturbations have a negligible effect on the temperature distribution in the interior.

The density perturbations to the equation of state are estimated using the additive volume law,

$$V(P,T) = V_H(P,T) + V_{He}(P,T) + V_Z(P,T), \tag{2}$$

where the total volume V is the sum of partial volumes of the main components V_H and V_{He}, the heavy element component V_Z. Hubbard & Militzer (2016) demonstrated that this leads to a modified density ρ in terms of the original H-He EOS density ρ_0,

$$\frac{\rho_0}{\rho} = \frac{1-Y-Z}{1-Y_0} + \frac{ZY_0 + Y - Y_0}{1-Y_0}\frac{\rho_0}{\rho_{He}} + Z\frac{\rho_0}{\rho_Z}, \tag{3}$$

in which all densities are are evaluated at the same $T(P)$ and Y_0 is the helium fraction used to calculate the H-He equation of state.

The choice of equation of state effects the density structure of the planet, and consequently, the distribution of heavy elements that is consistent with observational constraints. For comparison, we also construct models using the Saumon et al. (1995) equation of state (SCvH) for H-He mixtures, which has been used extensively in giant planet modeling.

Ab initio simulations show that, at the temperatures relevant to Jupiter's interior, there is no distinct, first-order phase transition between molecular (diatomic, in-

sulating) hydrogen to metallic (monatomic, conducting) hydrogen (Vorberger et al. 2007). In the context of a planet-wide model, however, the transition takes place over the relatively narrow pressure range between ∼1-2 Mbar. Within a similar pressure range an immiscible region opens in the H-He phase diagram Morales et al. (2013), which under correct conditions allows for a helium rain layer Stevenson & Salpeter (1977b,a). By comparing our adiabat calculations to the Morales et al. (2013) phase diagram, we predict such a helium rain layer in present-day Jupiter (Hubbard & Militzer 2016). The extent of this layer in our models is highlighted in Figure 1. While the detailed physics involved with the formation and growth of a helium rain layer is poorly understood, the existence of a helium rain layer has a number of important consequences for the large-scale structure of the planet. In our models, we assume this process introduces a superadiabatic temperature gradient and a compositional difference between the outer, molecular layer and inner, metallic layer.

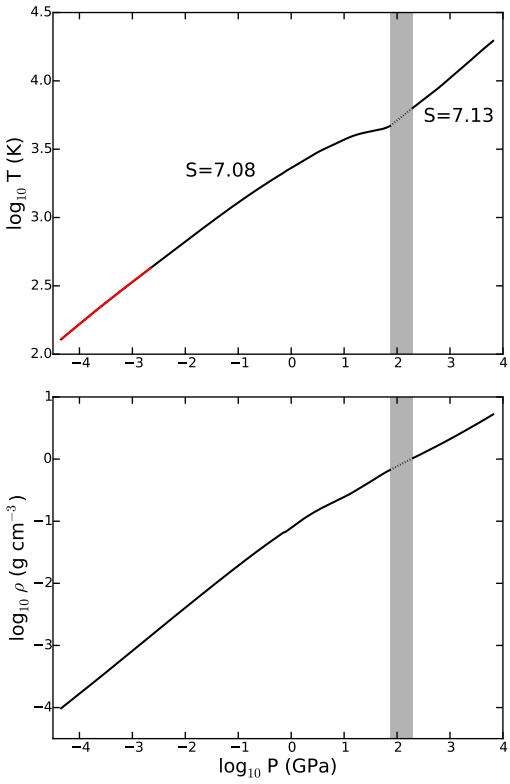

Figure 1. The barotrope used in preferred model Jupiter 'DFT-MD_7.13'. Top: temperature-pressure relationship for a hydrogen-Helium mixture with Y=0.245, with a entropy $S = 7.08$ at pressures below the demixing region, and $S = 7.13$ at pressures above the demixing region. The helium demixing region is shown by the gap and shaded region. The red line shows measurements from the *Galileo* probe. Bottom: density-pressure relationship for the same barotrope.

In summary, the barotrope and resulting suite of axisymmetric Jupiter models that we use in this investigation are identical to the results presented by Hubbard & Militzer (2016). Each model has a central core mass and envelope metallicities set to fit the observed J_2 (Jacobson 2003), with densities corrected to be consistent with non-spherical shape of the rotating planet. Since tidal corrections to a rotating Jupiter model are of order 10^{-7}, see Table 1 and the following section, it is unnecessary to re-fit the tidally-perturbed models to the barotrope assumed for axisymmetric models.

The physical parameters for each of these models is summarized in Table 2. The gravitational moments at the planet's surface are insensitive the precise distribution of extra heavy-element rich material within the innermost part of the planet. For instance, we cannot discern between dense rocky core with a and that same heavy material dissolved in metallic hydrogen and spread over a larger, but still restricted volume. Maintaining a constant core radius is computationally convenient when finding a converged core mass to J_2, since it requires no modification of the radial grid used through the envelope. For this reason we consider models with a constant core radius of $0.15a$. Decreasing this radius below $0.15a$ for a given core mass has a negligible effect on the calculated gravitational moments (Hubbard & Militzer 2016). Figure 2 shows the density profile for two representative models. In general, models using the DFT-MD equation of state lead to a larger central core and a lower envelope metallicity than those using SCvH. Hubbard & Militzer (2016) also noted that these models predict a value for J_4 outside the reported observational error bars (Jacobson 2003), since they would require unrealistic negative values of Z to match both J_2 and J_4.

3. STATIC TIDE CALCULATIONS

To calculate the gravitational moments, we use the non-perturbative *concentric Maclaurin spheroid* method which was introduced by Hubbard (2012, 2013) and extended to three dimensions by Wahl et al. (2016). In this method, the density structure is parameterized by N nested constant-density spheroids. For a given set of spheroids, the gravitational field is calculated as a volume-integrated function of all of the spheroids. The method then iterates to find the shape of each spheroid such that the surface of each is an equipotential surface under the combined effect of the planet's self-gravity, the centrifugal potential from rotation and the external gravitational perturbation from a satellite. The result is a model with self-consistent shape, internal density distribution and gravitational field described up to a chosen harmonic degree and order limit, $n_{\rm lim}$.

The non-spherical components of the gravitational po-

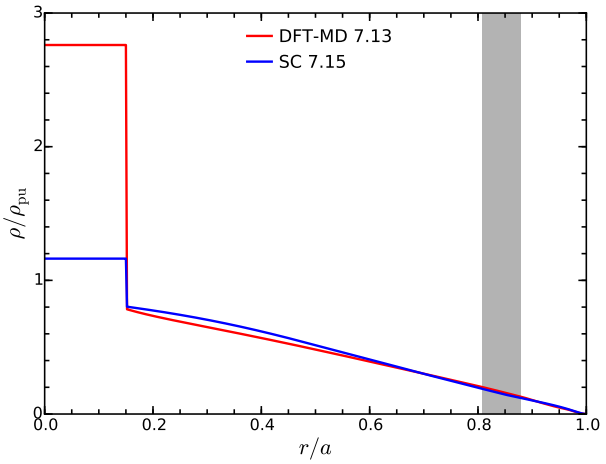

Figure 2. Density structure of Jupiter models (the planetary unit of density $\rho_{pu} = M/a^3$). The red curve shows our preferred model based on *ab initio* calculations. The blue curve uses the Saumon and Chabrier equation of state. The shaded area denotes the helium demixing region. Both models have $N = 511$ layers and a dense core within $r = 0.15a$. Constant core densities are adjusted to match J_2 as measured by fits to Jupiter flyby Doppler data (Jacobson 2003).

tential are described by two non-dimensional numbers

$$q_{\rm rot} = \frac{\omega^2 a^3}{GM}, \tag{4}$$

describing the relative strength of the rotational perturbation, and

$$q_{\rm tid} = -\frac{3m_{\rm s}a^3}{MR^3}, \tag{5}$$

the analogous quantity for the tidal perturbation. Here G is the universal gravitational constant, M is the total mass of the planet, a is the maximum equatorial radius, $m_{\rm s}$ is the mass of the satellite and R is the orbital distance of the satellite. The parameterization is completed by a third non-dimensional number R/a, representing the ratio of satellite distance to equatorial radius. For non-zero $q_{\rm tid}$, the calculated figure changes from a axisymmetric about the rotational axis to a fully triaxial spheroid.

From our CMS simulations, we find the zonal J_n and tesseral C_{nm} and S_{nm} gravitational harmonics. These harmonics sample slightly different regions of the planet. Figure 3 show the relative weight of the contribution to the low order J_n and C_{nm} as a function of non-dimensional radius. In the case of Jupiter and the Galilean satellites, $q_{\rm rot} \gg q_{\rm tid}$, and tidal perturbations from multiple moons can be linearly superposed. Moreover, all of the gravitationally important moons have orbits with nearly zero inclination. This allows us to treat a simplified case where we consider a single satellite with a fixed position in the equatorial plane, at angular coordinates $\mu = \cos\theta = 0$ (where θ is the satellite's colatitude measured from Jupiter's pole), and $\phi = 0$ (the satellite's Jupiter-centered longitude). By symmetry, this configuration constrains $S_{nm} = 0$, and the tidal Love numbers can then be determined from

$$k_{nm} = -\frac{2}{3}\frac{(n+m)!}{(n-m)!}\frac{C_{nm}}{P_n^m(0)q_{\rm tid}}\left(\frac{a}{R}\right)^{2-n}, \tag{6}$$

where $P_n^m(0)$ is the associated legendre polynomial evaluated at $\mu = 0$. In this paper we perform independent calculations for the three satellites with the largest $q_{\rm tid}$: Io, Europa and Ganymede (see Table 1).

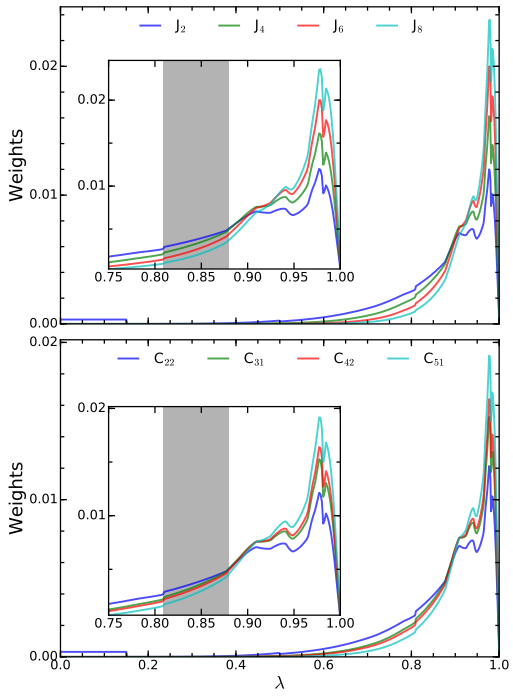

Figure 3. Top: Relative contribution of spheroids to external gravitational zonal harmonic coefficients up to order 8. Bottom: Relative contribution of spheroids to to external gravitational tesseral coefficients up to order 4. Tesseral moments of the same order (i.e. C_{31} and C_{33}) have indistinguishable radial distributions. Values normalized so that each harmonic integrates to unity. The shaded area denotes the helium demixing region.

For a tidally-perturbed non-rotating body, k_{nm} is degenerate with respect to m. However, Wahl et al. (2016) found that a large rotational bulge breaks this degeneracy. This leads to unexpectedly large values for some of the higher order k_{nm}. In the case of a rapidly-rotating gas giant, the predicted splitting of the k_{nm} and shift of k_{22} is well above the expected uncertainty of *Juno* measurements.

4. RESULTS

4.1. *State Mixing for Static Love Numbers*

In the CMS method applied to tides, we calculate the tesseral harmonics C_{nm} directly, and the Love numbers k_{nm} are then calculated using Eq. 6. For the common

tidal problem where $q_{\rm tid}$ and $q_{\rm rot}$ are carried to first order perturbation only, this definition of k_{nm} removes all dependence on the small parameters $q_{\rm tid}$ and a/R, which is convenient for calculating the expected tidal tesseral terms excited by satellites of arbitrary masses at arbitrary orbital distances. However, the high-precision numerical results from our CMS tidal theory reveal that when $q_{\rm rot} \approx 0.1$, as is the case for Jupiter and Saturn, the mixed excitation of tidal and rotational harmonic terms in the external gravity potential has the effect of introducing a small but significant dependence of k_{22} on a/R; see Fig. 4. In the absence of rotation, the CMS calculations yield results without any state mixing, and the k_{nm} are, as expected, constant with respect to a/R. It is important to note this effect on the *static* Love numbers because, as we discuss below, dynamical tides can also introduce a dependence on a/R via differing satellite orbital frequencies.

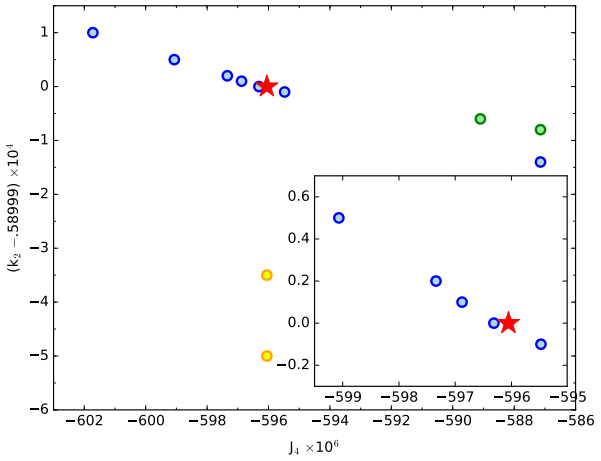

Figure 4. Predicted k_2 Love numbers for Jupiter models plotted against J_4. The favored interior model 'DFT-MD_7.13' with a tidal perturbation from Io is denoted by the red star. The other interior models with barotropes based on the DFT-MD simulations (blue) have k_2 forming a linear trend with J_4. Models using the Saumon and Chabrier barotrope (green) plot slightly above this trend. The of k_2 for a single model 'DFT-MD_7.13' with tidal perturbations from Europa and Ganymede (yellow) show larger differences than any resulting from interior structure.

4.2. *Calculated Static Tidal Response*

The calculated zonal harmonics J_n and tidal Love numbers k_{nm} for all of the Jupiter models with Io satellite parameters are shown in Tab. 3. Our preferred Jupiter model has a calculated k_2 of 0.5900. In all cases, these Love numbers are significantly different from those predicted for a non-rotating planet (see Tab. 4). Fig. 5 shows the different tesseral harmonics C_{nm} calculated with and without rotation. For a non-rotating planet with identical density distribution to the preferred model we find a much smaller $k_{22} = 0.53725$. *Juno* should, therefore, be able to test for the existence of the rotational enhancement of the tidal response.

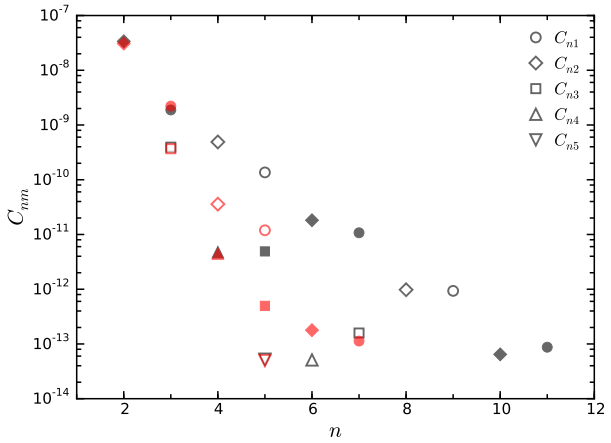

Figure 5. The tesseral harmonic magnitude C_{nm} for the 'DFT_MD 7.13' Jupiter model with a tidal perturbation corresponding to Io at its average orbital distance. Black: the values calculated with Jupiter's rotation rate; red: the values for a non-rotating body with identical layer densities. Positive values are shown as filled and negative as empty.

The effect of the interior mass distribution for a suite of realistic models has a minimal effect on the tidal response. Most models using the DFT-MD barotrope are within a 0.0001 range of values. The one outlier being the model constrained to match J_4 with unphysical envelope composition. The models using the SCvH barotrope yields slightly lower, but still likely indistinguishable values of k_{22}. The higher order harmonics show larger relative differences between models, but still below detection levels. Regardless, the zonal harmonic values are more diagnostic for differences between interior models than the tidal Love numbers. Fig. 4 summarizes these results, and shows that the calculated k_{22} value varies approximately linearly with J_4. If *Juno* measures higher order tesseral components of the field, it may be able to verify a splitting of the k_{nm} Love numbers with different m, for instance, a predicted difference between $k_{31} \sim 0.19$ and $k_{33} \sim 0.24$.

In addition, we find small, but significant, differences between the tidal response between Jupiter's most influential satellites. Fig. 6 shows the calculated C_{nm} for simulations with Io, Europa and Ganymede. We attribute the dependence on orbital distance to the state mixing described in Section 4.1. This leads to a difference in k_{22} between the three satellites (Tab. 4) that may be discernible in *Juno*'s measurements.

5. CORRECTION FOR DYNAMICAL TIDES

5.1. *Small Correction for Non-rotating Model of Jupiter*

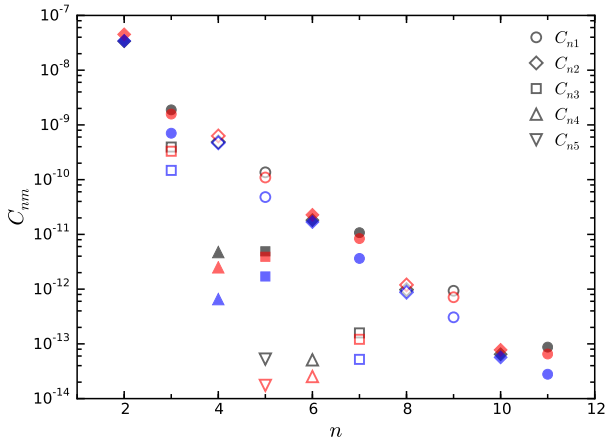

Figure 6. The tesseral harmonic magnitude C_{nm} for the 'DFT_MD 7.13' Jupiter model with a tidal perturbation corresponding to different satellites: Io (black), Europa (red) and Ganymede (blue).

The general problem of the tidal response of a rotationally-distorted liquid Jovian planet to a time-varying perturbation from an orbiting satellite has not been solved to a precision equal to that of the static CMS tidal theory of Wahl et al. (2016) and this paper. However, an elegant approach based on free-oscillation theory has been applied to the less general problem of a non-rotating Jovian planet perturbed by a satellite in a circular orbit (Vorontsov et al. 1984). Let us continue to use the spherical coordinate system (r, θ, ϕ), where r is radius, θ is colatitude and ϕ is longitude. Assume that the satellite is in the planet's equatorial plane ($\theta = \pi/2$) and orbits prograde at angular rate Ω_S. For a given planet interior structure, Vorontsov et al. (1984) first obtain its eigenfrequencies $\omega_{\ell mn}$ and orthonormal eigenfunctions $\mathbf{u}_{\ell mn}(r, \theta, \phi)$, projected on spherical harmonics of degree ℓ and order m (the index $n = 0, 1, 2, ...$ is the number of radial nodes of the eigenfunction). Note that in their convention, oscillations moving prograde (in the direction of increasing ϕ) have negative m, whereas some authors, e.g. Marley & Porco (1993) use the opposite convention.

Treating the tidal response as a forced-oscillation problem, equation (24) of Vorontsov et al. (1984), the vector tidal displacement ξ then reads

$$\xi(\mathbf{r}, t) = -\sum_{\ell,m,n} \frac{(\mathbf{u}_{\ell,m,n}, \nabla\psi^r_{\ell m})}{\omega^2_{\ell mn} - m^2\Omega_S^2} e^{-im\Omega_S t}, \qquad (7)$$

where $(\mathbf{u}_{\ell,m,n}, \nabla\psi^r_{\ell m})$ is the integrated scalar product of the vector displacement eigenfunction $\mathbf{u}_{\ell mn}(r, \theta, \phi)$ and the gradient of the corresponding term of the satellite's tidal potential $\psi^r_{\ell m}(r, \theta, \phi, t)$, *viz.*

$$(\mathbf{u}_{\ell,m,n}, \nabla\psi^r_{\ell m}) = \int dV \rho_0(r)(\mathbf{u}_{\ell,m,n} \cdot \nabla\psi^r_{\ell m}). \qquad (8)$$

The integral is taken over the entire spherical volume of the planet, weighted by the unperturbed spherical mass density distribution $\rho_0(r)$.

Vorontsov et al. (1984) then show that, for the nonrotating Jupiter problem, the degree-two dynamical Love number $k_{2,d}$ is determined to high precision ($\sim 0.05\%$) by off-resonance excitation of the $\ell = 2, m = 2, n = 0$ and $\ell = 2, m = -2, n = 0$ oscillation modes, such that

$$k_{2,d} = \frac{\omega^2_{220}}{\omega^2_{220} - (2\Omega_S)^2} k_2, \qquad (9)$$

noting that ω_{220} and ω_{2-20} are equal for nonrotating Jupiter (all Love numbers in the present paper written without the subscript d are understood to be static). For a Jupiter model fitted to the observed value of J_2, Vorontsov et al. (1984) set $\Omega_S = 0$ to obtain $k_2 = 0.541$, within 0.7% of our nonrotating value of 0.53725 (see Table 4). Setting Ω_S to the value for Io, Eq. 9 predicts that $k_{2,d} = 0.547$, i.e. the dynamical correction increases k_2 by 1.2%. This effect would be only marginally detectable by the *Juno* measurements of Jupiter's gravity, given the expected observational uncertainty.

5.2. *Dynamical Effects for Rotating Model of Jupiter*

For a more realistic model of Jupiter tidal interactions, the dynamical correction to the tidal response might be larger, and therefore, more detectable. We have already shown (Table 4) that inclusion of Jupiter's rotational distortion increases the static k_2 by nearly 10% above the non-rotating static value for a spherical planet. In this section, we note that Jupiter's rapid rotation may also change Jupiter's dynamic tidal response, by a factor that remains to be calculated.

In a frame co-rotating with Jupiter at the rate $\Omega_P = 2\pi/35730$s, the rate at which the subsatellite point moves is obtained by the scalar difference $\Delta\Omega = \Omega_S - \Omega_P$, which is negative for all Galilean satellites. Thus, in Jupiter's fluid-stationary frame, the subsatellite point moves retrograde (it is carried to the west by Jupiter's spin). For Io, we have $\Delta\Omega = -1.35 \times 10^{-4}$ rad/s. Jupiter's rotation splits the $\omega_{2\pm20}$ frequencies (Vorontsov & Zharkov 1981), such that $\omega_{2-20} = 5.24 \times 10^{-4}$ rad/s and $\omega_{220} = 8.73 \times 10^{-4}$ rad/s. The oscillation frequencies of the Jovian modes closest to tidal resonance with Io are higher than the frequency of the tidal disturbance in the fluid-stationary frame, but are closer to resonance than in the case of the non-rotating model considered by Vorontsov et al. (1984).

An analogous investigation for tides on Saturn raised by Tethys and Dione yields results similar to the Jupiter values: tides from Tethys or Dione are closer to resonance with normal modes for $\ell = 2$ and $m = 2$ and $m = -2$. Since our static value of k_2 for Saturn (Wahl et al. 2016) is robust to various assumptions about in-

terior structure and agrees well with the value deduced by Lainey et al. (2016), so far we have no evidence for dynamical tidal amplification effects in the Saturn system.

Unlike the investigation of Lainey et al. (2016), which relied on analysis of astrometric data for Saturn satellite motions, the *Juno* gravity investigation will attempt to directly determine Jupiter's k_2 by analyzing the influence of Jovian tesseral-harmonic terms on the spacecraft orbit. A discrepancy between the observed k_2 and our predicted static k_2 would indicate the need for a quantitative theory of dynamical tides in rapidly rotating Jovian planets.

6. CONCLUSIONS

Our study has predicted the static tidal Love numbers k_{nm} for Jupiter and its three most influential satellites. These results have the following features: (a) They are consistent with the most recent evaluation of Jupiter's J_2 gravitational coefficient; (b) They are fully consistent with state of the art interior models (Hubbard & Militzer 2016) incorporating DFT-MD equations of state, with a density enhancement across a region of H-He imiscibility (Morales et al. 2013); (c) We use the non-perturbative CMS method for the first time to calculate high-order tesseral harmonic coefficients and Love numbers for Jupiter.

The combination of the DFT-MD equation of state and observed J_{2n} strongly limit the parameter space of pre-*Juno* models. Within this limited parameter space, the calculated k_{nm} show minimal dependence on details of the interior structure. Despite this, our CMS calculations predict several interesting features of Jupiter's tidal response that the *Juno* gravity science system should be able to detect. In response to the rapid rotation of the planet the k_2 tidal Love number is predicted to be much higher than expected for a non-rotating body. Moreover, the rotation causes state mixing between different tesseral harmonics, leading to a dependence of higher order static k_{nm} on both m and the orbital distance of the satellite. An additional, significant dependence on a/r is expected in the dynamic tidal response. We present an estimate of the dynamical correction to our calculations of the static response, but a full analysis of the dynamic theory of tides has yet to be performed.

This work was supported by NASAs Juno project. Sean Wahl and Burkhard Militzer acknowledge the support the National Science Foundation (astronomy and astrophysics research grant 1412646).

REFERENCES

Archinal, B. A., A'Hearn, M. F., Bowell, E., et al. 2011, Celest. Mech. Dyn. Astron., 109, 101
Cao, H., & Stevenson, D. J. 2015, in Rev., arXiv:1508.02764
Gavrilov, S. V., & Zharkov, V. N. 1977, Icarus, 32, 443
Hubbard, W. B. 2012, Astrophys. J., 756, L15
—. 2013, Astrophys. J., 768, 43
Hubbard, W. B., & Militzer, B. 2016, Astrophys. J., 820, arXiv:1602.05143
Jacobson, R. A. 2003
Kaspi, Y. 2013, Geophys. Res. Lett., 40, 676
Kaspi, Y., Hubbard, W. B., Showman, A. P., & Flierl, G. R. 2010, Geophys. Res. Lett., 37, L01204
Lainey, V., Jacobson, R. A., Tajeddine, R., et al. 2016, Icarus (in Rev.), arXiv:1510.05870
Marley, M. S., & Porco, C. C. 1993, Icarus, 106, 508
Militzer, B. 2013, Phys. Rev. B, 87, 014202
Militzer, B., & Hubbard, W. B. 2013, Astrophys. J., 774, 148
Morales, M. a., Hamel, S., Caspersen, K., & Schwegler, E. 2013, Phys. Rev. B, 87, 174105
Perdew, J. P., Burke, K., & Ernzerhof, M. 1996, Phys. Rev. Lett., 77, 3865
Saumon, D., Chabrier, G., & van Horn, H. M. 1995, Astrophys. J. Suppl. Ser., 99, 713
Stevenson, D. J., & Salpeter, E. E. 1977a, Astrophys J Suppl., 35, 239
—. 1977b, Astrophys. J. Suppl. Ser., 35, 221
Vorberger, J., Tamblyn, I., Militzer, B., & Bonev, S. 2007, Phys. Rev. B, 75, 024206
Vorontsov, S. V., Gavrilov, S. V., Zharkov, V. N., & Leontev, V. V. 1984, Astron. Vestn., 18, 8
Vorontsov, S. V., & Zharkov, V. N. 1981, Sov. Astron., 25, 627
Wahl, S. M., Hubbard, W. B., & Militzer, B. 2016, Icarus (in Rev.), arXiv:1602.07350

Table 1. Jupiter Model Parameters

	Jupiter		
GM	1.26686535×10^8 [a]	(km^3/s^2)	
a	7.1492×10^4 [a]	(km)	
$J_2 \times 10^6$	14696.43 [a]		
$J_4 \times 10^6$	-587.14[a]		
q_{rot}	.08917920 [b]		
r_{core}/a	0.15		
	Io[b]	Europa[b]	Ganymede[b]
q_{tid}	-6.872×10^{-7}	-9.169×10^{-8}	-6.976×10^{-8}
R/a	5.90	9.39	14.98

References— a. Jacobson (2003), b. Archinal et al. (2011)

Table 2. Jupiter Model Values

	$S_{molec.}$ $(S/k_B/N_e)$	$S_{metal.}$ $(S/k_B/N_e)$	M_{core} (M_E)	$M_{Z,molec.}$ (M_E)	$M_{Z,metal.}$ (M_E)	Z_{global}
DFT-MD 7.24	7.08	7.24	12.5	0.9	10.3	0.07
DFT-MD 7.24 (equal-Z)	7.08	7.24	13.1	1.1	7.5	0.07
DFT-MD 7.20	7.08	7.20	12.3	0.8	9.9	0.07
DFT-MD 7.15	7.08	7.15	12.2	0.7	9.2	0.07
DFT-MD 7.15 (J_4)	7.08	7.15	9.7	-0.6	14.9	0.08
DFT-MD 7.13	**7.08**	**7.13**	**12.2**	**0.7**	**8.9**	**0.07**
DFT-MD 7.13 (low-Z)	7.08	7.15	14.0	0.2	1.1	0.05
DFT-MD 7.08	7.08	7.08	12.0	0.6	8.3	0.07
SC 7.15	7.08	7.15	4.8	3.5	28.2	0.11
SC 7.15 (J_4)	7.08	7.15	4.3	3.2	29.3	0.12

Model parameters fromHubbard & Militzer (2016). S is the specific entropy for the adiabat through the inner or outer H-He envelope. M is the mass of heavy elements included in each layer. Each model matches observed $J_2 = 14696.43 \times 10^6$ (Jacobson 2003), JUP230 orbit solution, to six significant figures. Models denoted as 'DFT-MD' if equation of state based on *ab initio* simulations or 'SC' for the Saumon et al. (1995) equation of state, with a number denoting the entropy below the helium demixing layer. The number of Models denoted with (J_4) also match observed $J_4 = -596.31 \times 10^{-6}$. Model denoted (equal-$Z$) is constrained to have same metallicity in inner and outer portions of the planet. Preferred interior model shown in bold face.

Table 3. Gravitational Harmonic Coefficients and Love Numbers

(all $J_n \times 10^6$)	J_4	J_6	J_8	J_{10}	k_{22}	k_{31}	k_{33}	k_{42}	k_{44}	k_{51}	k_{53}	k_{55}	k_{62}	k_{64}	k_{66}
pre-*Juno* observed	-587.14	34.25	...	...	...	...	...	...	...	...	...	...	...	...	...
(JUP230)[a]	±1.68	±5.22	...	...	...	...	...	...	...	...	...	...	...	...	...
DFT-MD 7.24	-597.34	35.30	-2.561	0.212	0.59001	0.19455	0.24424	1.79143	0.13920	0.98041	0.84803	0.09108	6.19365	0.52154	0.06451
DFT-MD 7.24 (equal-Z)	-599.07	35.48	-2.579	0.214	0.59004	0.19512	0.24498	1.79695	0.13984	0.98531	0.85239	0.09159	6.22719	0.52474	0.06492
DFT-MD 7.20	-596.88	35.24	-2.556	0.211	0.59000	0.19440	0.24404	1.78994	0.13902	0.97903	0.84678	0.09093	6.18392	0.52058	0.06438
DFT-MD 7.15	-596.31	35.18	-2.549	0.211	0.58999	0.19422	0.24381	1.78811	0.13881	0.97733	0.84526	0.09074	6.17202	0.51941	0.06423
DFT-MD 7.15 (J_4)	-587.14	34.18	-2.451	0.201	0.58985	0.19118	0.23989	1.75874	0.13537	0.95088	0.82162	0.08794	5.98975	0.50178	0.06195
DFT-MD 7.13	**-596.05**	**35.15**	**-2.546**	**0.210**	**0.58999**	**0.19413**	**0.24370**	**1.78728**	**0.13871**	**0.97655**	**0.84456**	**0.09066**	**6.16658**	**0.51887**	**0.06416**
DFT-MD 7.13 (low-Z)	-601.72	35.77	-2.608	0.217	0.59009	0.19599	0.24610	1.80546	0.14083	0.99296	0.85924	0.09239	6.28019	0.52985	0.06558
DFT-MD 7.08	-595.48	35.08	-2.539	0.210	0.58998	0.19395	0.24346	1.78542	0.13848	0.97482	0.84301	0.09047	6.15442	0.51767	0.06400
SC 7.15	-589.10	34.86	-2.556	0.214	0.58993	0.19112	0.24002	1.76641	0.13699	0.96568	0.83567	0.09024	6.12279	0.51832	0.06449
SC 7.15 (J_4)	-587.14	34.65	-2.534	0.212	0.58991	0.19048	0.23918	1.76013	0.13625	0.95997	0.83054	0.08963	6.08299	0.51443	0.06398

All Love numbers for a tidal response with $q_{\rm tid}$ and R/a corresponding to Jupiter's Satellite Io. Preferred interior model shown in bold face.

References—a. JUP230 orbit solution Jacobson (2003)

Table 4. Tidal Response for Various Satellites and Non-rotating Model

	Io	Io[a] non-rotating	Europa	Ganymede
k_{22}	**0.58999**	0.53725	0.58964	0.58949
k_{31}	**0.1941**	0.2283	0.1938	0.1937
k_{33}	**0.2437**	0.2283	0.2435	0.2435
k_{42}	**1.787**	0.1311	4.357	12.41
k_{44}	**0.1387**	0.1311	0.1386	0.1386
k_{51}	**0.9766**	0.0860	2.373	6.7486
k_{53}	**0.8446**	0.0860	2.0289	5.740
k_{55}	**0.0907**	0.0860	0.0906	0.0906
k_{62}	**6.167**	0.0610	37.04	302.1
k_{64}	**0.5189**	0.0610	1.237	3.487
k_{66}	**0.0642**	0.0610	0.0641	0.0641

Tidal response of preferred interior model 'DFT_MD 7.13' with $q_{\rm tid}$ and R/a for three large satellites, and for a 'non-rotating' model with $q_{\rm rot} = 0$. In bold face is the same preferred model as in 3.

[a] Non-rotating model has identical density structure to rotating model.